Discovery of novel inhibitor scaffolds against the metallo-β-lactamase VIM-2 by SPR based fragment screening

Tony Christopeit[1], Trine Josefine O. Carlsen[1], Ronny Helland[1] and Hanna-Kirsti S. Leiros[1]*

[1] The Norwegian Structural Biology Centre (NorStruct), Department of Chemistry, Faculty of Science and Technology, UiT The Arctic University of Norway, N-9037 Tromsø, Norway.

ABSTRACT

Metallo-β-lactamase (MBL) inhibitors can restore the function of carbapenem antibiotics and therefore help to treat infections of antibiotic resistant bacteria. In this study, we report novel fragments inhibiting the clinically relevant MBL VIM-2. The fragments were identified from a library of 490 fragments using an orthogonal screening approach based on a Surface Plasmon Resonance (SPR) based assay combined with an enzyme inhibition assay. The identified fragments showed IC_{50} values between 12 and 1500 μM and ligand efficiencies (LE) between 0.48 and 0.23 kcal/mol per heavy atom. For two of the identified fragments, crystal structures in complex with VIM-2 were obtained. The identified fragments represent novel inhibitor scaffolds and are good starting points for the design of potent MBL inhibitors. Furthermore, the established SPR based

assay and the screening approach can be adopted to other MBLs and in this way improve the drug discovery process for this important class of drug targets.

INTRODUCTION

The rapid emerging of antibiotic resistant bacteria is a major threat to global public health according to a report released by the World Health Organization (WHO) in 2014[1]. One of the last-line drugs for the treatment of patients infected with antibiotic resistant bacteria are carbapenem antibiotics. Disturbingly, an increasing number of carbapenemases, β-lactamases with a broad hydrolytic capacities to destroy carbapenem antibiotics, are reported[2]. Carbapenemases can be divided into two different groups, metallo-β-lactamases (MBL) and serine-β-lactamases (SBL)[3]. For SBLs, the co-administration of SBL inhibitors together with carabapenemen antibiotics has already been proven as a successful strategy to restore their function[4]. Despite the urgent need and the reporting of promising MBL inhibitors[5-9], so far there are no clinically approved drugs targeting MBL's [10].

One of the most clinically relevant MBL's is the Verona integron-encoded metallo-β-lactamase (VIM-2)[2]. The enzyme was first characterized in *Pseudomonas aeruginosa* [11], but has also spread to other bacteria like *Enterobacteriaceae*[12]. VIM-2 has a broad substrate hydrolysis range, including penicillins, cephalosporins, cephamycins, oxacephamycins, and carbapenems[11]. The enzyme is folded into a αβ/βα sandwich with two zinc ions in the active site bridged by a hydroxide ion[13]. Due to the high clinically relevance, the wide spread and the broad substrate range, VIM-2 is an important drug target to restore the function of carbapenem antibiotics and the treatment of antibiotic resistant bacteria.

Fragment based drug discovery (FBDD) is proven to have a high potential to identify novel inhibitor scaffolds especially for challenging drug targets. The method is based on identifying small molecule inhibitors with low affinity, which can be linked or further evolved into potent inhibitors. In this way, the chemical space can be explored more efficiently compared to traditional high-throughput screenings[14]. Different biochemical assays, e.g. enzymatic assays, and biophysical assays, e.g. NMR spectroscopy, X-ray crystallography, Surface plasmon resonance (SPR) spectroscopy, mass spectrometry and isothermal titration calorimetry have been adopted to the needs of FBDD[14]. A common problem in FBDD are false positive hits caused by Pan Assay Interference Compounds (PAINS)[15]. Such compounds show an apparent inhibition due to a variety of mechanisms, e.g. influencing assay conditions, interfering with read outs or unspecific binding to the protein surface. The use of an orthogonal screening approach, combining a biophysical and a biochemical assay, is the best way to avoid problems caused by PAINS[14]. Especially SPR based assays have a great potential to identify PAINS and hence are one of the most powerful screening techniques in FBDD[16-18]. Despite the clear advantage of the technique not only for FBDD, but also for hit to lead optimization, SPR based assays have rarely been used to study MBLs.

In this study, FBDD was used to identify novel inhibitor scaffolds, which have the potential to be further optimized into drug leads for the clinically relevant carbapenemase VIM-2. An SPR based assay was established for the enzyme and validated by studying the interaction with meropenem and captopril. An orthogonal screening approach combining a biophysical SPR based assay with a biochemical inhibition assay was used to screen a library of 490 fragments. 9 fragment specifically inhibiting VIM-2 were identified. For two of the fragments, detailed X-ray crystal structure were obtained. The structures allow identifying interactions crucial for the binding of the fragments.

RESULTS AND DISCUSSION

Expression, purification and characterization of VIM-2. The new His-tagged VIM-2 gene construct was expressed in *E. coli* and initially purified by immobilized metal ion affinity chromatography (IMAC). The His-tag was removed by cleavage using the tobacco etch virus (TEV) protease and the protein further purified by ion exchange chromatography. Protein identity was confirmed by mass spectroscopy and the protein purity was judged from the SDS-PAGE analyses to be above 95% (data not shown). Around 45 mg pure VIM-2 was yielded from 2 L cell culture.

Nitrocefin is a widely used chromogenic reporter substrate to monitor the activity of MBLs[10]. An enzyme activity assay based on nitrocefin was used to verify the activity of the purified VIM-2. Furthermore, the assay was used to explore the influence of different buffer conditions suitable for fragment screening and the DMSO concentration on the enzyme activity. Up to 2.5% DMSO, no influence on the enzyme activity was observed (data not shown). For the hydrolysis of nitrocefin, steady-state kinetic parameters K_m and k_{cat} were determined in HEPES buffer (pH 7.2) with 34 ± 2 μM and 1170 ± 25 s^{-1}, respectively (Figure 1A). Additionally, the IC$_{50}$ for the known MBL inhibitor captopril was determined to be 3.5 μM (Figure 1B). The values were in accordance with the literature[6, 19], showing that the chosen HEPES based buffer did not influence the activity of VIM-2 and hence was suitable to be used during the fragment screening.

SPR-based binding studies with meropenem and captopril. SPR based assays are widely used in drug discovery. However, such assays have rarely been used to study β-lactamases. We established an SPR based assay for VIM-2, suitable to study the interactions with small molecules. The immobilization of VIM-2 to the SPR sensor surface was achieved by biotin-streptavidin

capturing resulting in a stable surface with an immobilization level of around 1600 response units (RU). To ensure that the protein was active on the surface, the interactions with meropenem and captopril were investigated. Meropenem interacted reversibly with VIM-2, showing a fast association and dissociation (Figure 2A). The steady state values were calculated from the sensorgrams and plotted against the concentration. Data were fitted to a 1:1 interaction model and the binding affinity (K_D) was calculated with 12 μM. Due to the fast interaction kinetics, it was not possible to determine the association or dissociation constant. The determined K_D for meropenem was in a similar range as the K_m of 2 μM reported by *Docquier et. al.*[19]. Captopril bound reversibly to VIM-2 with a clear association and dissociation phase (Figure 2B). The sensorgrams could be described by a 1:1 interaction model. The calculated association constant (k_a) was $4.2*10^4 \, M^{-1}s^{-1}$, the dissociation constant (k_d) was $0.025 \, s^{-1}$ and K_D was 0.6 μM. The determined K_D was in accordance with the IC_{50} of 3.5 μM determined with enzymatic inhibition assay, showing that both assays produced consistent results. From the immobilization level of VIM-2 and the saturation levels reached by meropenem and captopril, it was estimated that around 35% of the immobilized protein were active. Although the signal intensity was in a low range, the interaction with captopril (Mw= 217.3 g/mol) clearly showed that the assay was capable to detect the binding of molecules in the size of fragments.

Screening of the fragment library. The aim of the study was to identify novel fragments inhibiting the metallo-β-lactamase VIM-2. The used fragment library was purchased from Maybridge (Cambridge, UK) and consisted of 490 fragments. All fragments had a molecular weight below 300, ≤ 3 H-bond acceptors and donors, ≤ 3 rotatable bonds and a clogP ≤ 3.

A common problem in fragment based drug discovery are false positive hits often caused by PAINS[15]. In this study, we choose an orthogonal screening strategy combining a biophysical and

a biochemical assay. It has been shown that such combination have high probability to avoid false positive hits [14]. The screening of the library was made in three consecutive steps, starting with a single concentration screening, followed by a concentration series screening and an inhibition screening.

The aim of the single concentration screening was to identify potentially binding fragments and to sort out fragments showing no interaction at all with VIM-2. The established SPR based biosensor assay was used to investigate the binding of all fragments at a single concentration of 300 μM. Repeated injections of captopril as positive controls insured that the surface was stable and VIM-2 was active during the whole screening. The screening was repeated two times in reversed sample orders. Sensorgrams were visually inspected to identify fragments inducing a significant signal increase in at least one of the screens. 53 fragments were selected for the concentration series screen.

The aim of the concentration series screen was to identify fragments causing false positive hits. Since SPR based assays can monitor fragment binding in real time, they have a great potential to identify such fragments[16]. The selected fragments from the single concentration screen were tested at four different concentration (300 μM, 100 μM, 33 μM and 11 μM). Sensorgrams were visually inspected and fragments showing extremely slow dissociation, strong secondary effects or no clear concentration dependency were rejected. Furthermore, for every fragment the theoretical R_{max} was calculated according to the signal of the positive control and the molecular weight of the fragment. Fragments showing at the highest concentration a signal five times higher as the theoretical maximum binding capacity (R_{max}) were rejected as promiscuous binders. Rejecting of fragments showing undesirable binding properties can result in false negative hits. However, it is unlikely and an accepted procedure in SPR based fragments screening to avoid problems caused by false

positive hits [16-18, 20, 21]. 27 fragments showed a concentration dependent reversible interaction with a K_D below 5 mM and a signal range expected for a 1:1 interaction. These fragments were further tested in the enzyme activity assay to determine their inhibition potency.

An SPR based assay gives only information about the binding of a fragment to a protein. Since the place of binding is unknown, it is not clear if such interactions have the ability to reduce the enzyme activity. Therefore, the fragments identified as binders in the single concentration screening and the concentration series screening were tested in an enzyme inhibition assay. 9 fragments showed at a concentration of 500 μM an inhibition of VIM-2 by more than 15% against nitrocefin and were hence considered as hits (Table 1). Several fragments identified as binders in the SPR based assay showed no or only weak inhibition. This can be caused by fragments binding outside of the active site and in this way not interfering with the substrate binding. Such fragments were not considered as interesting starting points for the inhibitor design.

Characterization of the fragment hits by determining the K_D and the IC_{50}. The SPR based assay was used to determine the K_D for the 9 fragment hits. All fragments were analyzed in a 1.5 dilution-series starting at 300μM (Figure 3). The steady state values were calculated from the sensorgrams, plotted against the concentration and fitted to an interaction model for a single binding site with a constant R_{max} (Table 1). Fragment **1** and **2** showed the highest K_D with 145 μM and 9 μM. These two fragments were also the only fragments showing a clear saturation in the steady state plots. However, it has been shown that steady state plots, also not reaching saturation, are a robust method to estimate K_D values [17].

The enzyme activity assay based on the substrate nitrocefin was used to determine the IC_{50} values for the fragment hits. For every fragment, the percentage of inhibition was determined in a 2-fold dilution series and plotted against the concentration (Figure 4). The IC_{50} values were

calculated by fitting the data to a one-parameter dose-response curve with a Hill coefficient of 1, a maximum activity of 100% and a minimum activity of 0% (Table 1). Due to high IC_{50} values and limited solubility, only parts of the dose-response curves were obtained and full inhibition could not be reached for several fragments. However, also in such cases the determined IC_{50} values can be assumed as good estimations sufficient for evaluating the fragment hits. Fragment **6** induced an increase in enzyme activity at the concentration 750 μM and 1500 μM. This was probably due to unspecific effects and hence the two highest concentrations were removed from the dose-response plot. Fragment **9** had a yellow color causing a strong background signal at higher concentrations. Therefore, the concentration 750 μM and 1500 μM were removed from the dose-response plot.

X-ray structures and structure activity relationship (SAR). To obtain structural information on the binding of the fragment hits, they were soaked into VIM-2 crystals. For fragment **1** and fragment **2**, complex structures were obtained clearly showing additional electron density in the active site of VIM-2 (Figure 6).

The complexes crystallized in the C2 space group with two protein molecules in the asymmetric unit or in I222 with one protein molecule in the asymmetric unit. Details on the X-ray data collection and refinement statistics are shown in Table 2. The obtained VIM-2 structures were similar to previous published structures [13, 22] with the typical αβ/βα sandwich folding and two Zn^{2+} ions located in the active site of the enzyme. The first Zn^{2+} (Zn1) was coordinated by His116, His118 and His169, whereas the second Zn^{2+} (Zn2) was coordinate by Asp120, Cys221 and His263. Both Zn ions were bridged by a hydroxide ion. A third Zn^{2+} (Zn3) was coordinated by His178 in one molecule, His285 of the symmetry mate and two chloride ions. In structure VIM-2-

1, one of the coordinating chloride ions was partially replaced by fragment **1**. The Zn3 binding site has been observed before in other VIM-2 structures [13, 22] and is likely a crystallographic artefact.

In the complex structure with fragment **1** and **2**, a partial oxidation of Cys221 to a cysteine sulfonate residue (Osc221) was observed. In order to prevent this oxidation, crystals were grown in the presence of 5 mM β-mercaptoethanol, 1 mM DTT or 1 mM TCEP. However, in our hands the additives had no influence on the degree of oxidation. To investigate the cause of oxidation further, data were collected at a low intensity beam at an in-house rotating anode radiation source. The structure showed no signs of oxidation of Cys221 (Figure 5). In contrast, data collected at the high intensity beamline BL14.1 at the BESSY II electron storage ring (Berlin-Adlershof, Germany) resulted in a structure with Cys221 completely oxidised to the cysteine sulfonate. Since the crystals used for both data collections were from the same 24 well crystallisation tray and had been grown for a similar amount of days, we suspect that oxidation of Cys221 was due to radiation damage[23, 24]. However, the overall structure of the oxidised and reduced form of VIM-2 were similar, except minor changes in the close environment of Cys221. Similar changes caused by oxidation of Cys221 have been observed before by *Garcia-Saez et. al.*[13] for VIM-2 and by *Borra et. al.* for VIM-7[25] and GIM-1[26].

In the structure VIM-2-**1** electron density corresponding to fragment **1** was observed in the active site of both molecules of VIM-2 (chain A and B) in the asymmetric unit (Figure 6). Fragment **1** directly interacted with the two Zn ions in the active site, whereby Zn1 was coordinated by the triazole ring and Zn2 by the thiol group. A positive difference in electron density was observed between the two zinc ions. This positive density was removed by adding a hydroxide ion bridging the two zinc ions. The occupancy for the bridging hydroxide ion was 0.22 and 0.32 (Chain A and B) and for the fragment 0.68 and 0.78 (Chain A and B). Furthermore, the hydroxide ion and

fragment **1** were in close contact. This indicates that the observed hydroxide ion is from the unbound native structure. Fragment **1** is already known as an inhibitor for the MBL IMP-1[27] and extensive SAR has been carried out, concluding that the thiol group is crucial for fragment binding, whereas the N-methyl group and the trifluoromethyl group did not influence the affinity[5]. Although the SAR studies have been carried out with IMP-1, they are in accordance with our VIM-2 crystal structures, showing that the N-methyl group and the trifluoromethyl group form no close interactions with the protein.

The experimental electron density map of structure VIM-2-**2** clearly showed the binding of fragment **2** to the active site of the two VIM-2 molecules (chain A and B) in the asymmetric unit (Figure 6). The carboxyl group of the fragment interacted with Zn2 and formed hydrogen bonds with two water molecules (W1 and W2) highly coordinated by the protein structure. A parallel π-π stacking with His263 and a T-shaped π-π stacking with Tyr67 was observed. The side chain of Arg228 showed a high mobility with different conformations partly forming hydrogen bond with the carboxyl group in the fragment. Additional hydrophobic interaction of the fluorine-substituted phenyl group with Phe61 and Trp87 stabilized the fragment binding. The carbonyl group of fragment **1** participated in two interactions, a hydrogen bond with Asn233 and the chelation of Zn1. However, the long distance between the carbonyl group and Zn1 (3.51 Å / 3.66 Å) indicates only a weak chelation. Furthermore, the carbonyl group favours the co-planar orientation of the two phenyl groups in the fragment and in this way enables the hydrophobic interactions with His263, Tyr67, Phe61 and Trp87. The exact interactions involved in the substrate binding of VIM-2 are not clear, since no crystal structure in complex with a substrate has been reported. However, it seems likely that the fragment mimics the carbapenem core structure and hence the interactions are similar as during substrate binding. This is further supported by the fact that binding of the

fragment did not displace the hydroxide ion bridging the two zinc ions, and normally has a role in attacking the substrate. The fluorine atom of fragment **2** showed no obvious interactions with the protein. To investigate if the fluorine atom was important for the binding of the fragment, the IC_{50} values were determined for two analogues of fragment **2**, one without the fluorine (**2a)** atom and one where the fluorine was replaced by chlorine atom (**2b)**. Removing fluorine slightly decreased the IC_{50} of the fragment, whereas the change to chlorine had no influenced on the on the IC_{50} of the fragment (Figure 7). This shows that the fluorine atom was not crucial for the binding affinity. In accordance with the crystal structure, removing of the carbonyl group (**2c)**, changing the carboxyl group into a methyl ester (**2d)** or removing of the fluorine-substituted phenyl group (**2e)** prevents important interactions and hence results in a strong increase of the IC_{50} values (Figure 7).

Although all fragment hits were soaked into VIM-2 crystals, only for fragment **1** and **2** convincing complex structures were obtained. The fact that no further complex structures were obtained might be explained by short soaking times and the low fragment concentration as well as the lower affinity of the fragments. However, optimisation of these factors was difficult due to the low stability of the crystals in solutions containing DMSO.

Evaluation of the fragment hits. The fragment hits identified in the screening showed a wide structural diversity and to our knowledge, none of them has been reported before as VIM-2 inhibitors. To evaluate the quality of the fragment hits, the ligand efficiency (LE) was calculated ranging from 0.48 to 0.23 kcal/mol per heavy atom (Table 1). LE is a common metric in FBDD and allows comparing the affinity of fragments corrected for their size. Fragments with a LE higher as 0.3 kcal/mol per heavy atom are normally considered as good starting points for further optimisation [28]. However, LE should not been seen as an absolute criteria and rather as an indicator, which can help to choose fragments most suitable for further optimisation.

Fragment **1** showed the highest ligand efficiency with 0.48 kcal/mol per heavy atom. The determined K_D and IC_{50} were 145 μM and 232 μM, respectively. This fragment has been previously identified during a fragment screening as an inhibitor of IMP-1[27] and several potent inhibitors for different MBLs containing fragment **1** have been recently reported [8]. However, these inhibitors have a potential to be further optimized and the structural information presented in this study will help to reach this task. Although rediscovering an already know fragment is disappointing, it clearly shows that the chosen screening approach is suitable to identify good starting points for the design of potent inhibitors.

Fragment **2** showed the lowest IC_{50} with 14 μM and a LE of 0.38 kcal/mol per heavy atom. The IC_{50} was further improved to 8 μM by removing the fluorine from the fragment (**2a**). To our knowledge, fragment **2** or his analogue **2a** have not been reported as inhibitor for MBL's. Due to the high affinity and the detailed structural information on the binding mode, the fragment is an ideal starting point for further optimisation into a potent inhibitor. Fragment **3** shows structural similarities to fragment **2**. Although no crystal structure of fragment **3** in complex with VIM-2 was obtained, it can be assumed that the carboxyl group and the carbonyl group of the fragment interact with the protein in a similar way as observed for fragment **2**. However, the lower ligand efficiency compared to fragment **2** makes the fragment less favourable for further optimisation.

Fragment **4** and **5** contain both a quinoline ring system as a scaffold. Quinoline ring systems have been reported before as part of MBL inhibitors[29]. Nevertheless, they have rarely been systematically explored for the design of potent inhibitors. Hence, fragment **4** with the higher LE compared to fragment **3**, offers an interesting starting point for the design of a potent quinoline based MBL inhibitor.

Fragment **6** contains 3-picolinic acid moiety. Different picolinic acid analogues have been reported as inhibitors for the MBL CphA[30]. CphA belongs to the B2 group of MBLs, containing only one Zinc ion in the active site. Hence, picolinic acid analogues could be interesting starting points for inhibitors targeting MBLs of different classes.

Fragment **8**, **7** and **9** showed LE around 0.3 and to our knowledge are novel scaffolds for the inhibition of MBLs. Although structural information about the exact binding mode were not obtained by X-ray crystallography, these fragments have a great potential for further optimisation into potent inhibitors.

CONCLUSION

MBL's are important drug targets to restore the function of carbapenem antibiotics and for the treatment of antibiotic resistant infections. So far, there are no MBL inhibitors in clinical use and hence, there is a clear need to identify novel starting points for the design of potent inhibitors. In this study, we used a fragment based approach to identify such starting points. We identified 9 novel fragments inhibiting VIM-2 with a K_D between 9 and 1500 μM and LE between 0.48 and 0.21 kcal/mol per heavy atom. For two of the identified fragments, crystals structures in complex with VIM-2 were obtained allow identifying the important interactions involved in the fragment binding. The fragment hits identified in this study and the obtained crystal structures will help to design novel MBL inhibitors and to improve already known ones.

The fragment based approached used in this study applied an SPR based assay and an enzyme inhibition assay. SPR based assays are widely used in drug discovery, but have rarely been used for β-lactamases. To our knowledge, this study is the first report using an SPR based assay to study an MBL. The SPR based assay and thereby the screening approach can easily be adapted to other

MBL's and in this way improve the drug discovery process for this important class of drug targets. The rediscovering of fragment **1** clearly shows that the screening approach established in this study is highly suitable to identify promising starting points for the development of potent inhibitors. Hence, the approach can be used to identify further interesting fragment hits by screening larger fragment libraries or more specialized libraries, like natural product based libraries or libraries with enhanced 3D characteristics.

EXPERIMENTAL SECTION

General Procedures. Chemicals and solvents were purchased from standard suppliers and used without further purification unless specified different. The fragment **2** analogues 2-benzoylbenzoic acid (**2a**), 2-(4-chlorobenzoyl)benzoic acid (**2b**), 2-benzylbenzoic acid (**2c**), methyl-2-benzoylbenzoate (**2d**), 2-acetylbenzoic acid (**2e**), were purchased from Sigma-Aldrich. Primers were purchased from Sigma-Aldrich. The class B β-lactamase numbering system is used throughout this paper for numbering of all residues [31].

Cloning, Expression and Purification of VIM-2. The *bla*VIM-2 gene was amplified from *Pseudomonas aeruginosa* strain 301-5473 and cloned into the expression vector pET26 (Novagen). The gene sequence coding for residues Val25 to Glu300 of VIM-2 was amplified from the template VIM-2 pET26 using Phusion PCR with the forward primer VIM-2-V25fw (5'-*CAT CAC CAT CAC CAT CAC* **GAA AAC CTG TAT TTC CAG GGA** gta gat tct agc gg- 3') and the reverse primer VIM-2rev (5'-<u>GGG GAC CAC TTT GTA CAA GAA AGC TGG GTC TTA</u> cta ctc aac gac tga gcg att -3', the TEV protease site is in bold, the 6xHis-tag in italic, gene specific parts in lower-case and the *att*B site is underlined). The PCR contained 1 x HF buffer, 200 μM deoxynucleoside triphosphate (dNTP) mix, 0.5 μM forward primer, 0.5 μM reverse primer,

approximately 100 ng VIM-2 pET26 template, 1 µL (0.02 U) Phusion polymerase and nuclease free water. The amplification started with an initial denaturation at 95°C for 5 min, followed by 30 cycles of denaturation at 95°C for 30 s, annealing at 55°C for 30 s and elongation at 72°C for 45 s, followed by a final extension at 72°C for 5 min. The PCR product was analysed by agarose gel electrophoresis and gel purified using the NucleoSpin Gel and PCR Clean-up kit (Macherey-Nagel).

After purification, the PCR product was used as a template in a second Phusion PCR conducted under the same conditions as described above. As forward primer *att*B1-His fw (5'- G GGG AC A AGT TTG TAC AAA AAA GCA GGC TTC GAA GGA GAT AGA ACC ATG *CAT CAC CAT CAC CAT CAC* -3', the 6xHis-tag is in italic and the *att*B site is underlined) and as reverse primer VIM-2rev were used. The PCR product was analysed by agarose gel electrophoresis, purified and used for a BP recombination reaction (recombination between *att*B and *att*P sites) to produce an entry clone in the pDONR221 vector (Invitrogen). Sequencing was performed to confirm the cloning using the BigDye Terminator v3.1 technology (Applied Biosystems) and M13 primer. The entry clone was transferred to the pDest14 vector in an LR recombination reaction (recombination between *att*L and *att*R sites) and used to transform XL-1 Blue cells (Agilent Bioscience). The expression construct was isolated by plasmid preparation using the Wizard Plus SV Minipreps DNA Purification Systems (Promega).

For the protein expression, *E. coli* BL21 (DE3) cells (Invitrogen) were transformed with the pDest14 vector containing the new VIM-2 construct. The cells were cultured overnight in 5 mL LB- medium and transferred to 500 mL Terrific broth (TB) medium supplied with 50 mg/L kanamycin (Sigma-Aldrich). The culture was grown at 37°C until reaching the log phase and

induced with 0.4 mM isopropyl-β-D-thiogalactopyranoside (IPTG) over night at 20°C. Cells were harvested by centrifugation and stored at -80°C.

The cell pellets from 2 L culture were solubilized in 70 mL buffer A (50 mM Tris/HCl pH 7.2, 150 mM NaCl, 100 μM $ZnCl_2$ and SIGMAFAST™ Protease Inhibitor Cocktail) and lysed by sonication, followed by a centrifugation (25400 g, 4°C, 30 min) to remove insolubilities. The supernatant was applied to a 5 mL HisTrap HP column (GE Healthcare) and washed with 5% buffer B (50 mM Tris/HCl pH 7.2, 150 mM NaCl, 100 μM $ZnCl_2$ and 500 mM imidazole). Bound protein was eluted using a linear gradient from 5% to 100% buffer B. Fractions containing VIM-2 were identified by SDS-PAGE and pooled. In-house produced His-tagged TEV protease [32] was added to the pooled fractions in a molecular ratio 1:10 and dialysed over night at 4°C against buffer A using a 10 kDa cut-off SnakeSkin dialyse tubing (Thermo Scientific). To remove contamination, uncleaved protein and the His-tagged TEV protease, a second His Trap purification was performed as described above. The flow through was collected and dialysed against 50 mM Tris/HCl pH 7.2 and 100 μM $ZnCl_2$. For final purification, the protein was applied to a 5 mL anion exchange Hitrap Q column and eluted with linear gradient across 0 to 1 M NaCl.

Enzyme activity and inhibition. Enzyme activity measurements were carried out at 25°C using a SpectraMax M2^e (Molecular Devices) and 96-well plates. The buffer used in all experiments consisted of 100 mM HEPES, 150 mM NaCl, pH 7.2, 100 μM $ZnCl_2$ and 0.005% surfactant P-20, 2.5% DMSO, 20 μg/mL BSA. Data were analyzed using the software SoftMax Pro 5.2 (Molecular Devices) and GraphPad Prism 5 (GraphPad Software). All measurements were repeated at least three times.

Steady state measurements were used to determine K_m and k_{cat} for nitrocefin (Calbiochem). The substrate was dissolved in buffer in a 2-fold dilution series starting from 250 μM. The enzymatic

reaction was started by adding VIM-2 to a final concentration of 75 pmol. Cleavage of the substrate was followed by measuring the absorption at 482 nm every 17 s over 20 min. The initial velocity was determined and, K_m and k_{cat} were calculated from the resulting Michaelis-Menten plot.

The inhibition of VIM-2 by the fragments select during the SPR screening was determined using the enzymatic nitrocefin assay. Fragments were dissolved in buffer, mixed with VIM-2 and incubated for 5 min. The enzymatic reaction was started by adding nitrocefin to a final concentration of 3 μM. The final fragment concentration was 500 μM and the final enzyme concentration was 75 pmol. The absorption was measured at 482 nm every 17 s over 20 min. The initial velocity was determined and the percentage of enzyme inhibition was calculated in relation to a reference without fragment.

To determine the IC_{50} values, the inhibition of each fragment was determined as described above for a 2-fold dilution series starting at 1.5 mM. The inhibition values were plotted against the fragment concentration and the IC_{50} values were calculated fitting the data to a dose-response curve with constant top plateau (100%), a constant bottom plateau (0%) and a constant Hill slope of -1.

Fragment library. The library contained 490 fragments selected from the Ro3 library from Maybridge (Cambridge, UK). All fragments in the library had a clogP ≤ 3, the number of H-bond acceptors and donors was ≤ 3 and the number of rotatable bonds was ≤ 3. The purity of the fragments was $\geq 95\%$. The molecular weights of the fragments ranged between 80 and 300 Da. Fragments were dissolved at 150 mM in 100% DMSO and stored at 4°C.

SPR-based interaction analyses. Experiments were performed at 25°C using a Biacore T200 (GE Healthcare). The running buffer consisted of 100 mM HEPES pH 7.2, 150 mM NaCl, 100 μM ZnCl$_2$, 0.005% surfactant P-20 and 2.5% DMSO. For data analyses, the Biacore T200 evaluation

software 2.0 (GE Healthcare) was used. All sensorgrams were reference and blank subtracted. Running buffer was used for blank injections and bulk effects were corrected using solvent correction.

VIM-2 was immobilized using streptavidin-biotin capturing. For the biotinylation, VIM-2 was mixed in a 1:1 molar ratio with biotinamidohexanoic acid N-hydroxysuccinimide ester (Sigma-Aldrich) in 0.1 M phosphate buffer pH 7.2 and incubated at room temperature for 30 min. Unreacted biotinamidohexanoic acid N-hydroxysuccinimide ester was removed using an Amicon ultra centrifugal filter (Merck Killipore Ltd.) with a molecular cut off of 10 kDa.

Streptavidin (Sigma-Aldrich) was covalently coupled to a CM5 chip (GE Healthcare) by standard amine coupling. Therefore, streptavidin was dissolved in 10 mM Na-Acetate pH 4.8 at a concentration of 300 μg/mL and injected for 1200 s. Afterwards, biotinylated VIM-2 was injected for 240 s at a flow rate of 5 μL/min. The surface was blocked by injecting running buffer containing 0.2 μg/mL biotin (Sigma-Aldrich). A reference surface was prepared by immobilizing streptavidin directly followed by blocking with biotin.

For the interaction studies, meropenem (Sigma-Aldrich) and captopril (N-[(S)-3-Mercapto-2-methylpropionyl]-L-proline, Sigma-Aldrich) were dissolved in running buffer and injected in a two-fold dilution concentration series ranging from 100 μM to 0.2 μM. The association was followed for 180 s and the dissociation for 240 s. Before and after every concentration series, a blank was injected. For captopril, the sensorgrams were directly fitted to a 1:1 binding model to calculate k_a, k_d and K_D. For meropenem, the steady state values were calculated from the sensorgrams and plotted against the concentration. The data were fitted to single site binding model to calculate K_D.

For the single concentration screen, all fragments were diluted to 300 μM in running buffer and injected for 30 s. The dissociation was followed for 15 s. For every 12th fragment, a positive control containing 300 μM captopril and a blank were injected. Sensorgrams were visually inspected and fragments inducing a reversible signal increase above the noise level were selected for the secondary screening. The whole fragment library was screened two times in different orders.

Fragments selected in the single concentration screening were tested again in a concentration series of 900 μM, 300 μM, 100 μM, 33 μM and 11 μM. The fragments were diluted in running buffer and injected for 30 s. The dissociation was followed for 15 s. Before and after every concentration series a blank and a positive control of 300 μM captopril were injected. Fragments showing a concentration dependent interaction were selected for the inhibition screening. For every fragment, the theoretical R_{max} was calculated and adjusted to the signal of the positive control. Fragments showing signals 5 times higher as the theoretical R_{max} where discharged as promiscuous binders.

For determining the K_D of the fragment hits, a 1.5-fold dilution series starting from 300 μM was analysed. The association was followed for 30 s and the dissociation for 15 s. 300 μM captopril was used as positive control. The steady state values were extracted from the sensorgrams and plotted against the concentration. The binding affinity was estimated by fitting the data to a single site interaction model with a constant R_{max}. The R_{max} was adjusted according to the signal from the positive control and the molecular weight of the fragment.

Crystallisation, Soaking and Data Collection. VIM-2 was crystallized by the hanging drop method in 24-well plates by mixing 1 μl of the protein solution (10 mg/mL) with 1 μL reservoir solution. The concentrations in the reservoir were 22-27% poly ethylene glycol (PEG) 3350, 0.2 M magnesium formate and 5 mM β-mercaptoethanol. Crystals appeared after several days. For data

collection, the crystals were cryoprotected with 25% PEG 3350, 0.2 M $MgCl_2$, 15% ethylenglycol and 50 mM HEPES pH 7.2, and flash cooled in liquid nitrogen. To obtain structures in complex with the fragment hits, crystals were soaked for at 2 to 3 h in cryoprotecant containing each fragment (5 mM) prior to the freezing. X-ray diffraction data were collected on beamline ID29 at the European Synchrotron Radioation Facility (ESRF) in Grenoble, France, on BL14.1 operated by the Joint Berlin MX-Laboratory at the BESSY II electron storage ring (Berlin-Adlershof, Germany) [33] or at in-house rotating anode radiation source. Conditions for the data collection are shown in Table 2. The data set were integrated, scaled and truncated using XDS [34], POINTLESS and AIMLESS [35,36]. The phase problem was solved by molecular replacement with PHASER [37] using a VIM-2 structure (PDB ID:1KO3). Final structures were obtained by several refinement cycles using PHENIX [38]. Between the refinement cycles, manual model building in WinCoot [39] was used to optimize the model according to the $2F_0 - F_C$ and $F_0 - F_C$ electron density maps. Translation / Libration / Screw (TLS) parameters were used in the refinement process. Zn and Cl ions were anisotropically refined. Five percent of the X-ray data were used for R-free cross validation. The PyMOL Molecular Graphics System, Version 1.4.1 Schrödinger, LLC was used to generate illustrations. LIGPLOT[40] was used to visualize interaction.

FIGURES

Figure 1. (a) Steady-state kinetics for VIM-2 hydrolyses of nitrocefin. K_m was calculated with 34 ± 2 μM and k_{cat} with 1171 ± 25 s^{-1} (b) Dose-response curve for the inhibition of VIM-2 by captopril.

Figure 2. Sensorgrams for the interaction of (a) meropenem and (b) captopril with VIM-2. For meropenem, the steady state values were determined and plotted as a function of the concentration shown as inset. A single binding site model was fitted to the data to calculate K_D. For captopril, a 1:1 binding model was directly fitted to the sensorgrams (red lines).

Figure 3. Sensorgrams and steady state plots for the binding of the validated fragment hits to VIM-2. Fragments were tested in a 1.5 dilution series starting at 300 μM. Steady state values were calculated 5 s before the injection stopped and plotted against the concentration. The K_D was calculated by fitting the data to a single binding site model with a constant R_{max}.

Figure 4. Inhibition data for the fragment hits. Fragments were tested in a 2-fold dilution series starting at 1500 μM. The IC_{50} values were calculated by fitting the data to a dose-response curve with constant top plateau (100%), a constant bottom plateau (0%) and a constant Hill slope of -1.

Figure 5. Zn binding site of the (a) reduced and (b) oxidized form of VIM-2. Data for the reduced structure were collected at an in-house radiation source using a rotating anode. Data for the oxidized structure were collected at beamline BL14.1 at the synchrotron facility BESSY II (Berlin-Adlershof). The electron density map $2F_0\text{-}F_C$ (blue) around residue 221 is shown at 1σ. The difference maps $F_0\text{-}F_C$ are shown at 4 σ (green) and -4 σ (red). Zn ions are shown in orange and water molecules in red.

Figure 6. X-ray structure of fragment **1** (a and c; VIM-1-**1**) and fragment **2** (b and d; VIM-1-**2**) bound to the active site of VIM-2. The complexes crystallized with two copies in the asymmetric unit. Fragment carbon atoms are depicted in blue and VIM-2 carbon atoms in green. Water molecules are shown in red, Zn^{2+} in orange and hydroxide ions in purple. The final $2F_0$-F_c map around the ligand is shown in blue at 1σ. The difference maps F_0-F_c around the ligand are shown at 4σ (green) and -4σ (red). In (a), the hydroxide ion bridging the two Zn^{2+} is not shown, since it was assumed that it was an artefact from the native structure without bound fragment **1**. LIGPLOT[40] was used to analyze the interactions of fragment **1** (e) and fragment **2** (f). Hydrogen bonds are shown as red dashed lines and inter-atomic distances are given in Å (taken from the interaction with chain A). Hydrophobic interactions are indicated by a red arc.

Figure 7. Structure and inhibition data of the fragment **2** analogues. Fragments were tested in a 2-fold dilution series starting at 1500 μM. The IC_{50} were calculated by fitting the data to a dose-response curve with constant top plateau (100%), a constant bottom plateau (0%) and a constant Hill slope of -1.

Figure 1.
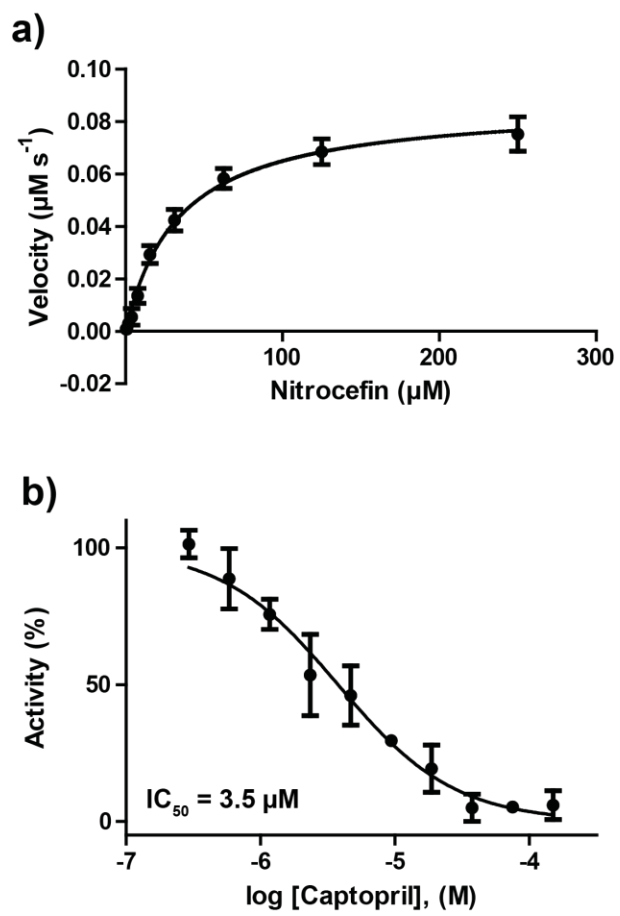
Figure 2.
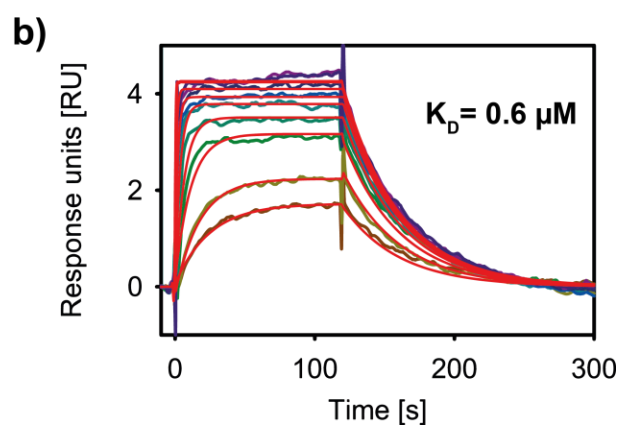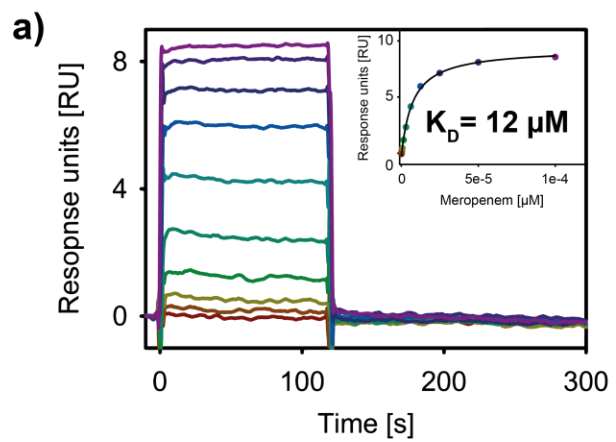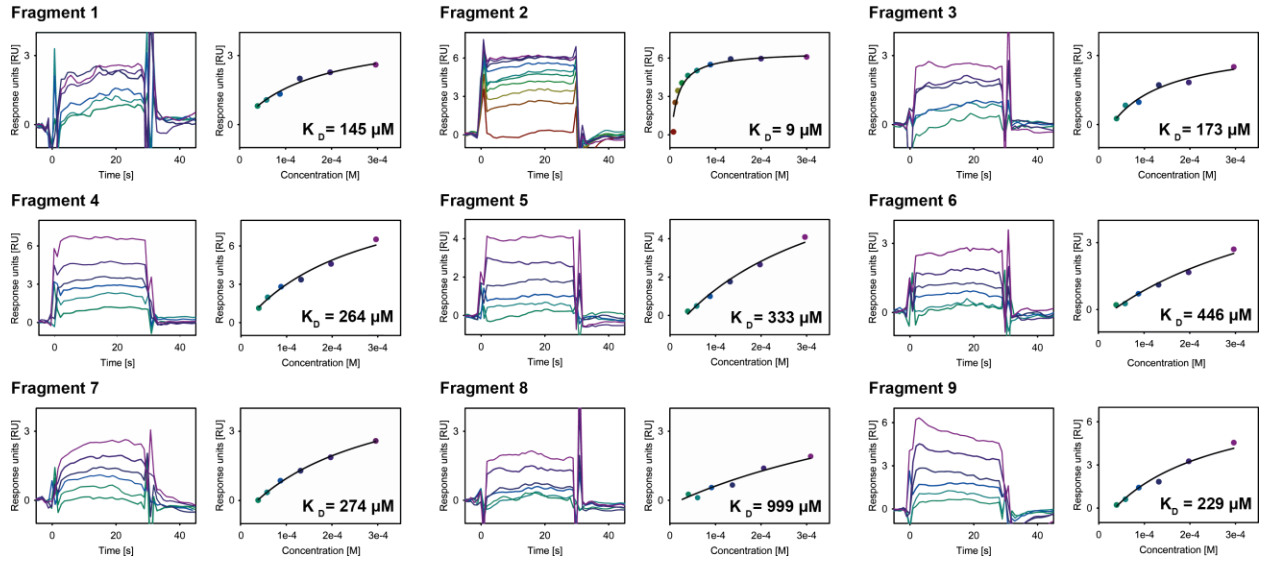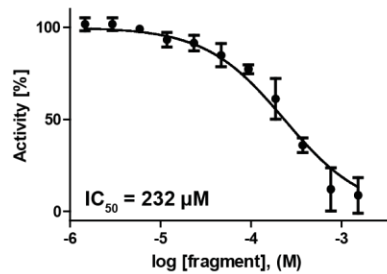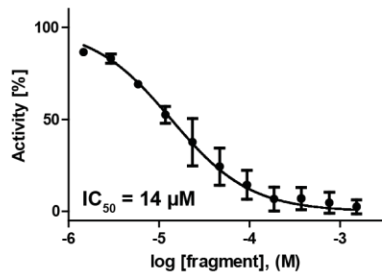
a)

b)

Figure 3.

Fragment 1 … $K_D = 145\ \mu M$

Fragment 2 … $K_D = 9\ \mu M$

Fragment 3 … $K_D = 173\ \mu M$

Fragment 4 … $K_D = 264\ \mu M$

Fragment 5 … $K_D = 333\ \mu M$

Fragment 6 … $K_D = 446\ \mu M$

Fragment 7 … $K_D = 274\ \mu M$

Fragment 8 … $K_D = 999\ \mu M$

Fragment 9 … $K_D = 229\ \mu M$
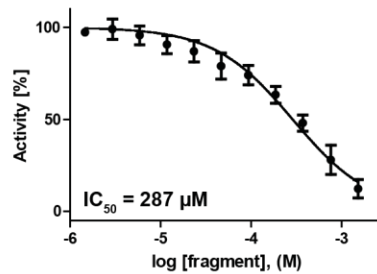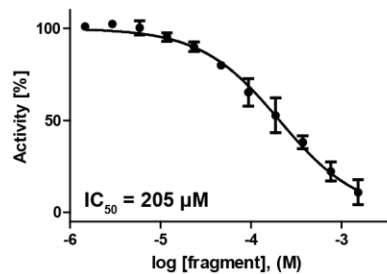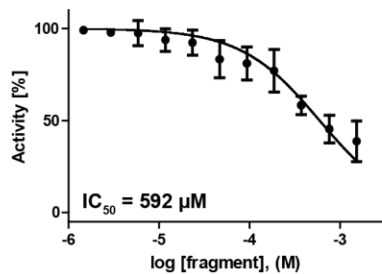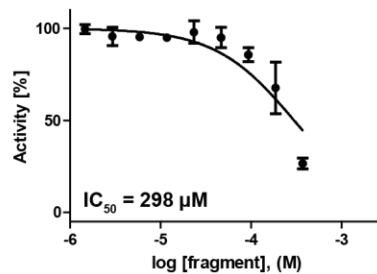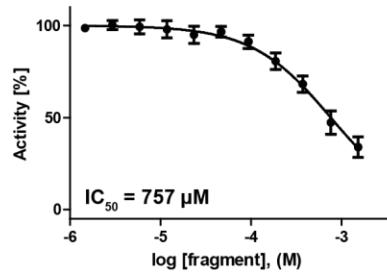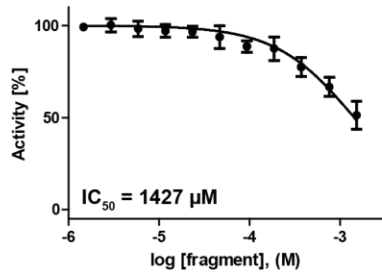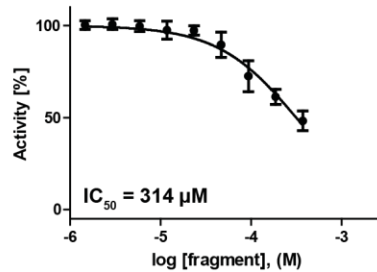
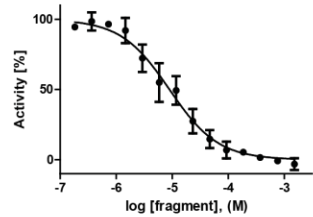**Figure 4.**

Figure 5.

a) VIM-2-NAT

b) VIM-2-OX

Figure 6.

VIM-2-**1**   VIM-2-**2**
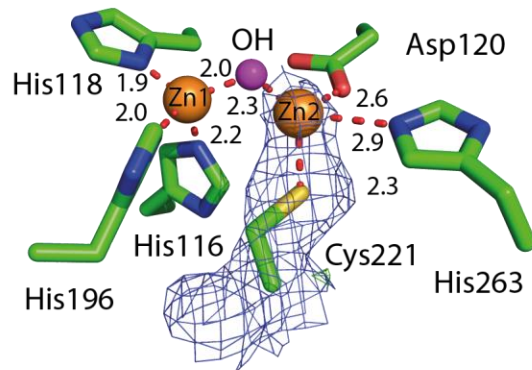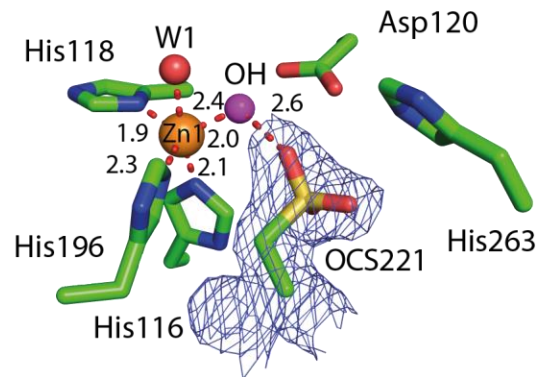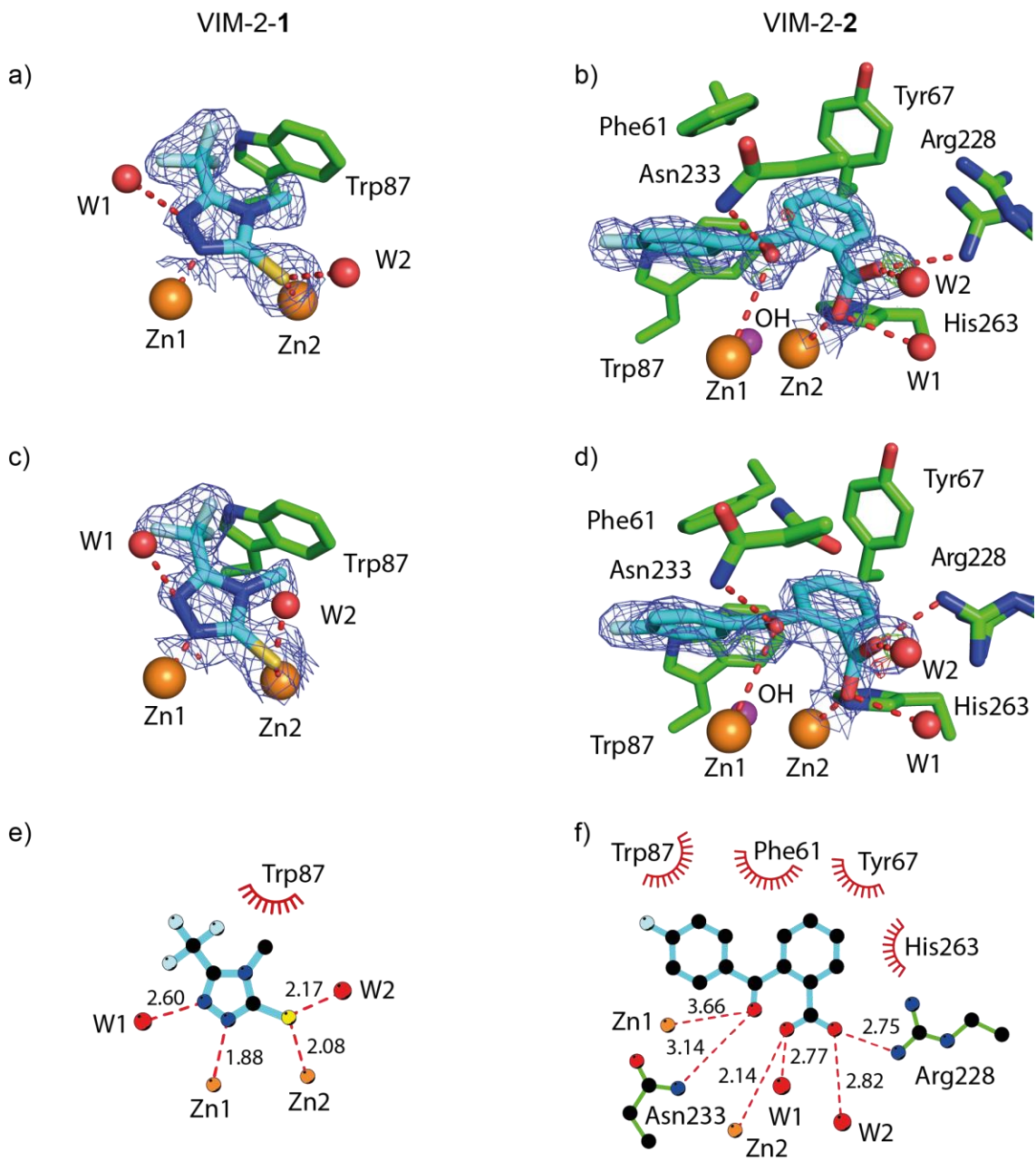
Figure 7.

Fragment 2a
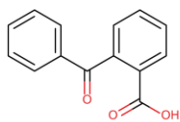
IC$_{50}$ = 8 μM

Fragment 2b
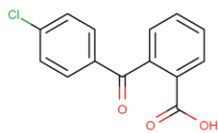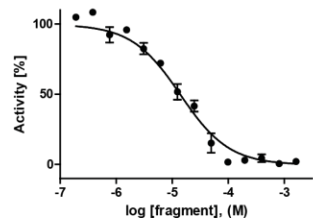
IC$_{50}$ = 12 μM

Fragment 2c
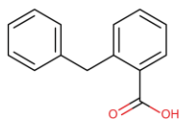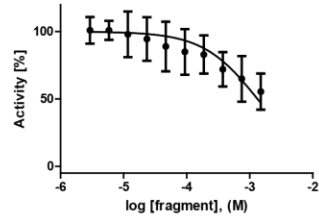
IC$_{50}$ > 1 mM

Fragment 2d
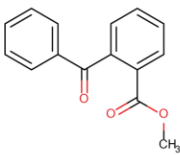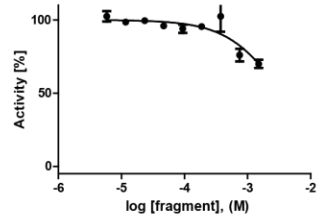
IC$_{50}$ > 3 mM

Fragment 2e
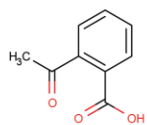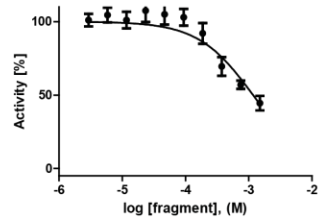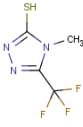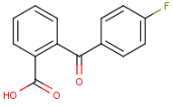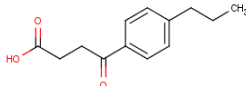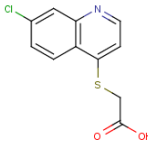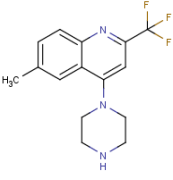
IC$_{50}$ > 1 mM

TABLES

Table 1. Molecular structure, binding affinity (K_D), inhibition constant (IC_{50}) and ligand efficiency (LE) for the identified fragment hits.

Table 2. X-ray data collection and refinement statistics for VIM-2-NAT, VIM-2-OX, VIM-2-**1** and VIM-2-**2**

Table 1.
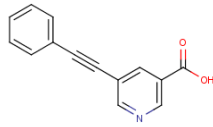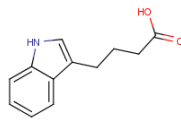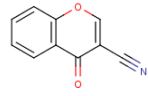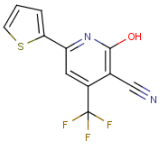
Fragment	Structure	K_D [μM][a]	IC_{50} [μM][a]	Ligand efficiency (LE)[b]
1		145	232	0.48
2		9	14	0.38
3		173	287	0.32
4		264	205	0.31
5		333	592	0.23
6		446	298	0.27
7		274	757	0.32
8		999	1427	0.31
9		229	314	0.28

[a] Logarithmic values and standard deviations are reported in the supporting material. [b] Ligand efficiencies were calculated as LE = (-R*T*lnK_D)/(number of heavy atoms) and are reported in kcal/mol per heavy atom

Table 2.

Parameter	VIM-2-NAT	VIM-2-OX	VIM-2-**1**	VIM-2-**2**
PDB entry	5ACU	5ACV	5ACW	5ACX
Data collection statistics				
Beamline	Rotating anode	BL14.1	ID29	ID29
Space group	I222	C2	C2	C2
Molecules in asymmetric unit	1	2	2	2
Unit cell dimensions				
a, b, c, Å	64.42, 75.80, 79.29	100.71 79.48 66.84	101.54, 79.29, 67.92	101.23, 79.22, 67.64
$\gamma°$		129.2	130.3	130.2
No. of unique reflections	11392	26390	37595	37523
Resolution, Å (highest bin)	24.96-2.10 (2.31-2.10)	25.63-1.96 (2.01-1.96)	38.72 – 1.80 (1.85- 1.80)	39.61-1.80 (1.85-1.80)
Wavelength, Å	1.5418	0.91840	0.97625	0.97625
Completeness, %	97.7 (97.0)	91.2 (88)	98.8 (94.0)	99.1 (99.0)
Multiplicity	3.7 (3.9)	3.7 (3.5)	4.6 (4.8)	4.6 (4.5)
Mean $<I>/<\sigma I>$	14.2 (5.3)	26.5 (8.1)	15.2 (3.2)	7.1 (4.6)
Willson B-factor, Å^2	25.44	16.84	14.80	16.97
R_{merge}, %	6.2 (22.7)	5.5 (20.1)	6.7 (37.2)	9.9 (19.3)
Refinement statistics				
R_{work}/R_{free} (%)	25.74/28.69	16.17/20.94	14.17/18.95	14.44/19.25
No. of atoms				
Protein	1747	3637	3664	3688
Ligand	-	-	44	36
Water	94	599	674	616
Other	$1OH^-$, $3Zn^{2+}$, $2Cl^-$	$2OH^-$, $6Zn^{2+}$, $4Cl^-$	$2OH^-$, $6Zn^{2+}$, $4Cl^-$	$2OH^-$, $6Zn^{2+}$, $4Cl^-$
Avg B-factor				
Protein	39.63	20.65	21.23	23.72
Ligand (occupancy)	-	-	33.64 (0.78/0.68/0.67/0.69)	42.54 (1.0/1.0)
Water	34.19	29.50	32.33	33.23
RMSD				
Bond length (Å)	0.003	0.003	0.009	0.004
Bond angle (°)	0.672	0.759	1.172	0.892

ASSOCIATED CONTENT

Supporting Information.

Logarithmic values and standard deviation for the values shown in Table 1. This material is available free of charge via the Internet at http://pubs.acs.org.

Accession codes.

Coordinates and structure factors of VIM-2-NAT, VIM-2-OX, VIM-2-**1** and VIM-2-**2** have all been deposited in the Protein Data Bank with accession numbers 5ACU, 5ACV, 5ACW and 5ACX.

AUTHOR INFORMATION

Corresponding Author

*E-mail: hanna-kirsti.leiros@uit.no. Phone: (+47) 776 45706

Author Contributions

Conceived and designed the experiment: HKSL TC. Performed the experiments: TC TJOC HKSL RH. Analyzed the data: TC HKSL. Wrote the paper: TC HKSL. All authors have given approval to the final version of the manuscript.

Notes

The authors declare no competing financial interest

ACKNOWLEDGMENT

ABBREVIATIONS

PAINS, pan assay interference compounds; VIM-2, verona integron-encoded metallo-β-lactamase 2; SPR, surface plasmon resonance; HEPES, 2-(4-(2-Hydroxyethyl)-1-piperazinyl)-ethansulfonsäure; RU, response units; DMSO, dimethyl sulfoxide; LE, ligand efficiency; MBL, metallo-β-lactamase; FBDD, Fragment based drug discovery; IMAC, immobilized metal ion affinity chromatography; PDB, Protein Data Bank; TEV, tobacco etch virus; SDS-PAGE, sodium dodecyl sulfate polyacrylamide gel electrophoresis; K_D, binding affinity; k_a, association constant; k_d, dissociation constant; SBL, serine-β-lactamase; LE, Ligand efficiency; Mw, molecular weight; R_{max}, maximum binding capacity;

REFERENCES

1. WHO. *Antimicrobial resistance: global report on surveillance 2014*; 2014.
2. Nordmann, P.; Naas, T.; Poirel, L. Global spread of Carbapenemase-producing Enterobacteriaceae. *Emerg Infect Dis* **2011,** 17, 1791-8.
3. Queenan, A. M.; Bush, K. Carbapenemases: the versatile β-lactamases. *Clin Microbiol Rev* **2007,** 20, 440-58, table of contents.

4.   Drawz, S. M.; Bonomo, R. A. Three decades of β-lactamase inhibitors. *Clin Microbiol Rev* **2010,** 23, 160-201.

5.   Faridoon; Hussein, W. M.; Vella, P.; Islam, N. U.; Ollis, D. L.; Schenk, G.; McGeary, R. P. 3-mercapto-1,2,4-triazoles and N-acylated thiosemicarbazides as metallo-β-lactamase inhibitors. *Bioorg Med Chem Lett* **2012,** 22, 380-6.

6.   Klingler, F. M.; Wichelhaus, T. A.; Frank, D.; Cuesta-Bernal, J.; El-Delik, J.; Muller, H. F.; Sjuts, H.; Gottig, S.; Koenigs, A.; Pos, K. M.; Pogoryelov, D.; Proschak, E. Approved Drugs Containing Thiols as Inhibitors of Metallo-β-lactamases: Strategy To Combat Multidrug-Resistant Bacteria. *J Med Chem* **2015,** 58, 3626-30.

7.   Feng, L.; Yang, K. W.; Zhou, L. S.; Xiao, J. M.; Yang, X.; Zhai, L.; Zhang, Y. L.; Crowder, M. W. N-heterocyclic dicarboxylic acids: broad-spectrum inhibitors of metallo-β-lactamases with co-antibacterial effect against antibiotic-resistant bacteria. *Bioorg Med Chem Lett* **2012,** 22, 5185-9.

8.   Zhang, Y. L.; Yang, K. W.; Zhou, Y. J.; LaCuran, A. E.; Oelschlaeger, P.; Crowder, M. W. Diaryl-substituted azolylthioacetamides: Inhibitor discovery of New Delhi metallo-β-lactamase-1 (NDM-1). *ChemMedChem* **2014,** 9, 2445-8.

9.   King, A. M.; Reid-Yu, S. A.; Wang, W.; King, D. T.; De Pascale, G.; Strynadka, N. C.; Walsh, T. R.; Coombes, B. K.; Wright, G. D. Aspergillomarasmine A overcomes metallo-β-lactamase antibiotic resistance. *Nature* **2014,** 510, 503-6.

10. Fast, W.; Sutton, L. D. Metallo-β-lactamase: inhibitors and reporter substrates. *Biochim Biophys Acta* **2013,** 1834, 1648-59.

11. Poirel, L.; Naas, T.; Nicolas, D.; Collet, L.; Bellais, S.; Cavallo, J. D.; Nordmann, P. Characterization of VIM-2, a carbapenem-hydrolyzing metallo-β-lactamase and its plasmid- and integron-borne gene from a *Pseudomonas aeruginosa* clinical isolate in France. *Antimicrob Agents Chemother* **2000,** 44, 891-7.

12. Livermore, D. M.; Woodford, N. The β-lactamase threat in Enterobacteriaceae, Pseudomonas and Acinetobacter. *Trends Microbiol* **2006,** 14, 413-20.

13. Garcia-Saez, I.; Docquier, J. D.; Rossolini, G. M.; Dideberg, O. The three-dimensional structure of VIM-2, a Zn-β-lactamase from *Pseudomonas aeruginosa* in its reduced and oxidised form. *J Mol Biol* **2008,** 375, 604-11.

14. Zartler, E.; Shapiro, M. Designing a Fragment Process to Fit Your Needs. In *Fragment-based drug discovery: a practical approach*, John Wiley & Sons: Chichester, U.K., 2008.

15. Baell, J. B.; Holloway, G. A. New substructure filters for removal of pan assay interference compounds (PAINS) from screening libraries and for their exclusion in bioassays. *J Med Chem* **2010,** 53, 2719-40.

16. Giannetti, A. M.; Koch, B. D.; Browner, M. F. Surface plasmon resonance based assay for the detection and characterization of promiscuous inhibitors. *J Med Chem* **2008,** 51, 574-80.

17. Giannetti, A. M. From experimental design to validated hits a comprehensive walk-through of fragment lead identification using surface plasmon resonance. *Methods Enzymol* **2011,** 493, 169-218.

18. Navratilova, I.; Hopkins, A. L. Fragment screening by surface plasmon resonance. *ACS Med Chem Lett* **2010,** 1, 44-8.

19. Docquier, J. D.; Lamotte-Brasseur, J.; Galleni, M.; Amicosante, G.; Frere, J. M.; Rossolini, G. M. On functional and structural heterogeneity of VIM-type metallo-β-lactamases. *J Antimicrob Chemother* **2003,** 51, 257-66.

20. Geitmann, M.; Elinder, M.; Seeger, C.; Brandt, P.; de Esch, I. J.; Danielson, U. H. Identification of a novel scaffold for allosteric inhibition of wild type and drug resistant HIV-1 reverse transcriptase by fragment library screening. *J Med Chem* **2011,** 54, 699-708.

21. Elinder, M.; Geitmann, M.; Gossas, T.; Kallblad, P.; Winquist, J.; Nordstrom, H.; Hamalainen, M.; Danielson, U. H. Experimental validation of a fragment library for lead discovery using SPR biosensor technology. *J Biomol Screen* **2011,** 16, 15-25.

22. Aitha, M.; Marts, A. R.; Bergstrom, A.; Moller, A. J.; Moritz, L.; Turner, L.; Nix, J. C.; Bonomo, R. A.; Page, R. C.; Tierney, D. L.; Crowder, M. W. Biochemical, mechanistic, and spectroscopic characterization of metallo-β-lactamase VIM-2. *Biochemistry* **2014,** 53, 7321-31.

23. Ravelli, R. B.; Leiros, H. K.; Pan, B.; Caffrey, M.; McSweeney, S. Specific radiation damage can be used to solve macromolecular crystal structures. *Structure* **2003,** 11, 217-24.

24. Leiros, H. K.; Timmins, J.; Ravelli, R. B.; McSweeney, S. M. Is radiation damage dependent on the dose rate used during macromolecular crystallography data collection? *Acta Crystallogr D Biol Crystallogr* **2006,** 62, 125-32.

25. Borra, P. S.; Leiros, H. K.; Ahmad, R.; Spencer, J.; Leiros, I.; Walsh, T. R.; Sundsfjord, A.; Samuelsen, Ø. Structural and computational investigations of VIM-7: insights into the substrate specificity of vim metallo-β-lactamases. *J Mol Biol* **2011,** 411, 174-89.

26. Borra, P. S.; Samuelsen, Ø.; Spencer, J.; Walsh, T. R.; Lorentzen, M. S.; Leiros, H. K. Crystal structures of Pseudomonas aeruginosa GIM-1: active-site plasticity in metallo-β-lactamases. *Antimicrob Agents Chemother* **2013,** 57, 848-54.

27. Vella, P.; Hussein, W. M.; Leung, E. W.; Clayton, D.; Ollis, D. L.; Mitic, N.; Schenk, G.; McGeary, R. P. The identification of new metallo-β-lactamase inhibitor leads from fragment-based screening. *Bioorg Med Chem Lett* **2011,** 21, 3282-5.

28. Schultes, S.; de Graaf, C.; Haaksma, E. E. J.; de Esch, I. J. P.; Leurs, R.; Krämer, O. Ligand efficiency as a guide in fragment hit selection and optimization. *Drug Discovery Today: Technologies* **2010,** 7, e157-e162.

29. Jin, W.; Arakawa, Y.; Yasuzawa, H.; Taki, T.; Hashiguchi, R.; Mitsutani, K.; Shoga, A.; Yamaguchi, Y.; Kurosaki, H.; Shibata, N.; Ohta, M.; Goto, M. Comparative study of the inhibition of metallo-β-lactamases (IMP-1 and VIM-2) by thiol compounds that contain a hydrophobic group. *Biol Pharm Bull* **2004,** 27, 851-6.

30. Horsfall, L. E.; Garau, G.; Lienard, B. M.; Dideberg, O.; Schofield, C. J.; Frere, J. M.; Galleni, M. Competitive inhibitors of the CphA metallo-β-lactamase from Aeromonas hydrophila. *Antimicrob Agents Chemother* **2007,** 51, 2136-42.

31. Garau, G.; Garcia-Saez, I.; Bebrone, C.; Anne, C.; Mercuri, P.; Galleni, M.; Frere, J. M.; Dideberg, O. Update of the standard numbering scheme for class B β-lactamases. *Antimicrob Agents Chemother* **2004,** 48, 2347-9.

32. Leiros, H. K.; Skagseth, S.; Edvardsen, K. S.; Lorentzen, M. S.; Bjerga, G. E.; Leiros, I.; Samuelsen, Ø. His224 alters the R2 drug binding site and Phe218 influences the catalytic efficiency of the metallo-β-lactamase VIM-7. *Antimicrob Agents Chemother* **2014,** 58, 4826-36.

33. Mueller, U.; Darowski, N.; Fuchs, M. R.; Forster, R.; Hellmig, M.; Paithankar, K. S.; Puhringer, S.; Steffien, M.; Zocher, G.; Weiss, M. S. Facilities for macromolecular crystallography at the Helmholtz-Zentrum Berlin. *J Synchrotron Radiat* **2012,** 19, 442-9.

34. Kabsch, W. Xds. *Acta Crystallogr D Biol Crystallogr* **2010,** 66, 125-32.

35. Evans, P. Scaling and assessment of data quality. *Acta Crystallogr D Biol Crystallogr* **2006,** 62, 72-82.

36. Evans, P. R. An introduction to data reduction: space-group determination, scaling and intensity statistics. *Acta Crystallogr D Biol Crystallogr* **2011,** 67, 282-92.

37. McCoy, A. J.; Grosse-Kunstleve, R. W.; Adams, P. D.; Winn, M. D.; Storoni, L. C.; Read, R. J. Phaser crystallographic software. *J Appl Crystallogr* **2007,** 40, 658-674.

38. Adams, P. D.; Afonine, P. V.; Bunkoczi, G.; Chen, V. B.; Davis, I. W.; Echols, N.; Headd, J. J.; Hung, L. W.; Kapral, G. J.; Grosse-Kunstleve, R. W.; McCoy, A. J.; Moriarty, N. W.; Oeffner, R.; Read, R. J.; Richardson, D. C.; Richardson, J. S.; Terwilliger, T. C.; Zwart, P. H. PHENIX: a comprehensive Python-based system for macromolecular structure solution. *Acta Crystallogr D Biol Crystallogr* **2010,** 66, 213-21.

39. Emsley, P.; Lohkamp, B.; Scott, W. G.; Cowtan, K. Features and development of Coot. *Acta Crystallogr D Biol Crystallogr* **2010,** 66, 486-501.

40. Wallace, A. C.; Laskowski, R. A.; Thornton, J. M. LIGPLOT: a program to generate schematic diagrams of protein-ligand interactions. *Protein Eng* **1995,** 8, 127-34.